Arch. Metall. Mater. **64** (2019), 4, 1257-1261

DOI: 10.24425/amm.2019.130088

WEI WANG*,**#, WEIJIE CHEN*,**

RAMAN SPECTROSCOPY STUDIES OF CARBON-BASED CATHODE MATERIALS DURING ALUMINUM ELECTROLYSIS

The sodium expansion and creep strain of semi-graphitic cathodes are investigated using a modified Rapoport apparatus. To further understanding of the sodium and bath penetration damage processes, the impact of external stress fluence on the carbon cathode microstructure has been defined with XRD analysis, Raman spectroscopy and scanning electron microscope (SEM). Graphite atoms fracture into smaller fragments that are less directional than the pristine platelets, which allows for a possible filling of the cracks that thus develop by the sodium and bath during aluminum electrolysis. The average microcrystalline size (calculated by Raman spectroscopy) is reduced by the deformation. The decreased intensity and widened 'G' and 'D' peaks in the analysis indicate the poor order of the sheets along the stacking direction while the consistent layered graphite structure is sustained.

Keywords: Aluminum electrolysis; Carbon cathode; Raman spectroscopy; Creep deformation; Sodium expansion

1. Introduction

Aluminum production has been carried out by the Hall-Heroult process for more than 100 years. An aluminum reduction cell, consisted of various structural materials, is specifically designed for aluminum production [1]. Currently, there is an effort to prolong the service life of the cell to decrease the power consumption and lower negative environmental effects [2]. More attention is paid to the relation between the damage of carbon cathodes and the life-determining procedure for cells. Expansion of cathode materials, arising from sodium penetration and intercalation with carbon, causes degradation of the cathode and contributes to premature cell shutdown [3-5]. During aluminum electrolysis, the compressive damage of the cathode can be attributed to the deterioration of the carbon structure, which results in the development of slip planes, kink bands and large quantities of dislocated walls [6,7]. However, the changes of the crystal defects and lattice parameters of the hexagonal crystal in carbon cathodes are not fully understood.

Raman spectroscopy has been successfully used to determine the average size of the crystalline domains in graphite [8,9]. Markervich et al. provided a detailed explanation of how the average grain size of the graphite electrodes (calculated by Raman spectroscopy) decreases as cycling progresses [10]. Krishna et al. intensively studied the influence of electron radiation on the crystal parameters of graphite and found that the decreased intensity and widened 'G' and 'D' peaks in the test results have a close relationship with the turbulence and the poor order of the sheets along the stacking direction [11]. Fillers, binders, pores, cracks, turbulence and quinoline insoluble particles are microstructural components that are observed in graphite and their reaction to stress dramatically influences the observed Raman features.

To investigate the deformation mechanism of the carbon cathode and improve the cell design, we supplemented the Rapoport-Samoilenko-type test with Raman spectroscopy and SEM analysis to clarify the influence of deformation on the lattice parameters of graphite. The results could provide insight into the microstructure and the deformation mechanism of the carbon cathode.

2. Experimental

2.1. Materials and chemicals

Industrial grade cryolite, NaF, CaF_2, and Al_2O_3 were used as analytical reagents obtained from Wongjiang Reagent (Guangdong, China), and the purity was higher than 99.8%. The chemicals used in this work were fully dried in a drying furnace with P_2O_5 at 200°C for at least 4 hours before aluminum electrolysis. In every experiment, the total weight of the chemicals was 180 g with 4% Al_2O_3 and 5% CaF_2 at a NaF/AlF_3 molar ratio of ~2.5.

Graphite (65%) and electrocalcined anthracites (35%) were blended with a given constant amount of the liquid binder pitches prepared beforehand. The mixture was molded in a liquid press-

* COLLEGE OF MATERIALS SCIENCE AND ENGINEERING, HENAN UNIVERSITY OF SCIENCE AND TECHNOLOGY, LUOYANG 471023, CHINA.
** COLLABORATIVE INNOVATION CENTER OF NONFERROUS METALS HENAN PROVINCE, LUOYANG 471023, CHINA.
# Corresponding author: wwlyzwkj@126.com

ing experimental facility with rated pressure of 22 MPa and was formed into a circular column with the dimensions of 25 mm in diameter and 50 mm in length. Three green samples were dried at 150°C. The samples were then heated up to 1200°C in a corundum crucible filled with unused carbonaceous blocks. Sample 2 was used to investigate sodium expansion and sample 3 was for creep strain.

2.2. Experimental procedure

The experimental apparatus and routine for deformation measurement of the carbon cathode were similar to those reported previously [6]. A thin nitride disk was laid between the anode (a carbon crucible) and the cathode (an experimental specimen of ∅25×50 mm) in the electrolytic tank for electrical insulation. Thus, the direct current passed from the positive pole to the anode guide rod, the side of the carbon crucible, the melt, the cathode investigated and finally to the negative electrode. The carbon crucible was placed into an electric heating furnace and was fixed to the anode rod by a flange ring. The top of the experimental cathode specimen was covered with the cathode lead using electrode paste. The sodium expansion and creep deformation of the test sample during electrolysis were recorded by a LVD (Linear Variable Differential) sensor (extent 10 mm, resolution 1 μm) set on top of the heater. The outside pressure was supplied using a dynamic device, which could keep the pressure at a constant value fora an extended period. The electrolysis was performed with the current density of cathode of 0.45 A/cm^2. Generally, only the axial strain is concerned, so the relation between displacement /time and strain/time could be defined using Eq. (1).

$$\varepsilon = \frac{h_t - h_0}{h_0} \tag{1}$$

where h_0 represents the original coordinates of the test sample and h_t represents the coordinates of the test sample for the corresponding test time.

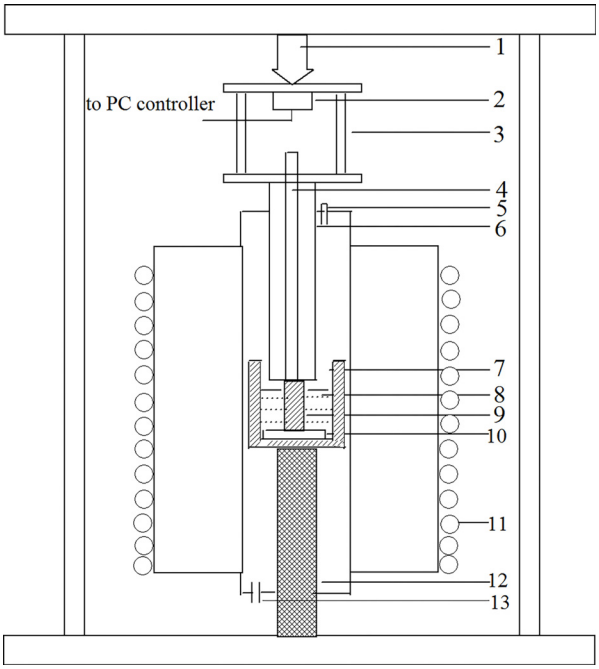

Fig. 1. Schematics of apparatus for measuring the sodium expansion and creep during aluminum electrolysis: (1) outside force (2) transducer (3) load transfer box (4) locating rod (5) gas outlet (6) load transfer rod (7) carbon crucible (8) melt (9) test specimen (10) insulation film (11) resistance wire (12) connecting rod (13) gas inlet

2.3. Sample characterization

Raman spectroscopy is a standard nondestructive tool to evaluate any structural changes after sodium expansion and creep deformation. A Renishaw in Via Raman spectrometer with Ar-gon-Kr laser source (with the 514.5 nm emitting lines, 0.2 mW) and focused by a Leica microscope (numerical aperture 0.75) was used for the test. The measurements were conducted under a low-density laser power (1-5 mW) to avoid overheating and oxidation of the testing sample. Each individual spectrum was fitted to asymmetric Lorentzian peaks by a least-squares fitting routine, from which the peak positions, linewidths, and integrated intensities of the Stokes lines at 1345 cm^{-1} (disorder-induced) and 1575 cm^{-1} (graphite) were determined. The morphology of the testing samples was observed before and during the experiment using SEM (JSM-5610LV microscope).

3. Results and discussion

3.1. Sodium expansion and creep strain

Fig. 2 (a) and Fig. 2 (b) show the curves of sodium expansion and plastic strain of the samples during laboratory electrolysis against operating time, respectively, with the cryolite ratio of 2.5 at 950°C. Over the course of 20 minutes from the start time, the sodium expansion of the cathode sample increased quickly. As the testing was conducted, the expansion rate declined gradually and finally reached a constant value. The results were similar for the creep strain.

One can state that the penetration of the sodium and bath mass during aluminum electrolysis has a close relationship with the internal graphite structure degradation. To evaluate any variations in the fine structure of the carbon cathode, XRD analysis, SEM imaging and Raman spectroscopy were used.

3.2. XRD analysis and raman spectroscopy of carbon cathode microstructure

Fig. 3 shows the XRD characterization of the carbon cathode before and after electrolysis. Sample 1 indicated a considerable C (002) peak at 2θ = 26.38°, which corresponded to a characteristic interlayer spacing d_{002} of 3.376 Å. However, after sodium expansion, the C (002) peak of Sample 2 was moved to

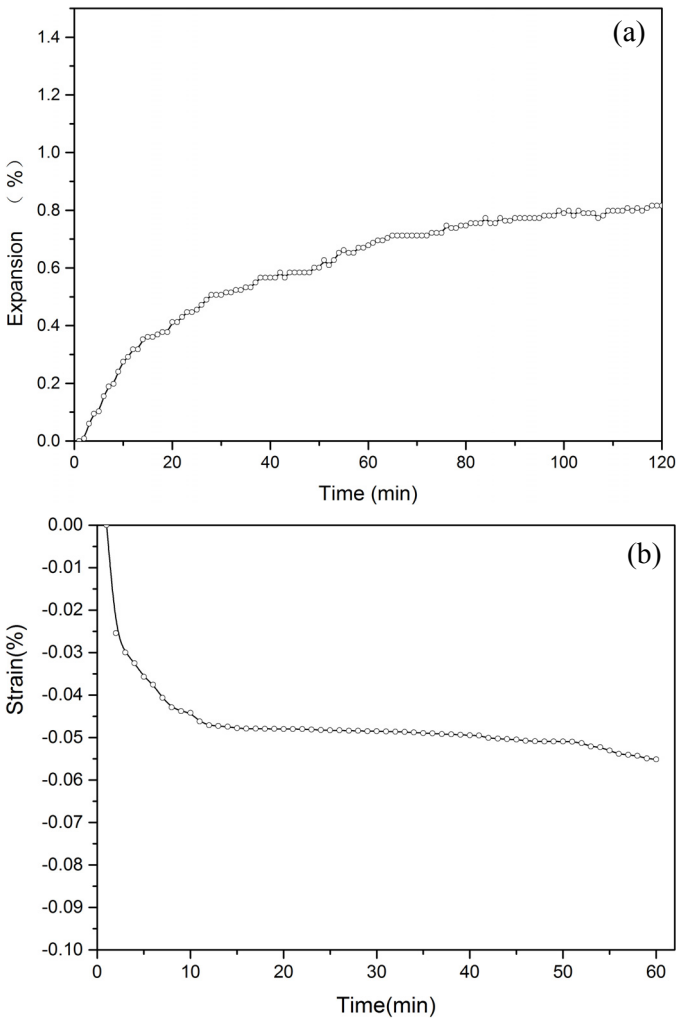

Fig. 2. Sodium expansion and plastic strain of the cathode specimen in the process of aluminum electrolysis (950°C, 0.5 A/cm^2). (a) Sodium expansion and (b) creep strain (loading pressure: 5 MPa)

the lower angle, 26.10°. According to the Bragg's law [6], the interlayer spacing (d_{002}) of Sample 2 was 3.411 Å. The larger interlayer spacing of Sample 2 was attributed to sodium penetration and intercalation with carbon. Instead, after creep deformation, the interlayer spacing (d_{002}) of Sample 3 was reduced to 3.341 Å, which may due to the the graphite layers restacking under stress.

Raman spectroscopy is a key diagnostic tool that has been used to identify various carbon-based materials (including graphite) and monitor carrier density, defects, and strain [12-14]. The peak with a broad and intense band originates from the in-plane vibrational E_{2g} phonon and locates at approximately 1580 cm^{-1}, is referred to as the G peak, and is associated with the bond stretching of C-C bonds in sp^2-hybridized carbon. Disordered carbons and polycrystalline graphite display an additional peak around 1350 cm^{-1} (A_{1g} mode, D peak), which is attributed to the disorder associated with finite crystallite sizes [15,16]. The 2D band (2738 cm^{-1}) is the second order of the D band, which is caused by a two-phonon double resonance [17, 18]. Furthermore, the ratio between the intensities of D band and G band (I_D/I_G) can accurately evaluate the extent of disorder in graphite structures. The mean in-plane crystallite domain size L_a (Å) could be calculated according to the following equation [12].

$$L_a = 43.5\left(\frac{I_D}{I_G}\right)^{-1} \quad (2)$$

Fig. 4 shows representative Raman spectra of three carbon cathodes. The peak positions, full width at half maximum (FWHM) of the G peak and the intensity ratio $I_{(D)}/I_{(G)}$ from these spectra can serve as a measurable tool for carbon cathodes. The intensity ratio $I_{(D)}/I_{(G)}$ was calculated for the pristine carbon cathode (sample 1) and the deformed carbon cathodes (sample 2 and sample 3) as a mean value for five various points on the basal plane surfaces of relatively big carbon cathodes. The FWHM of the G band in the sample 1 was less than 30 cm^{-1} and the ratio R was much less than unity, as is presented in Table 1. Both sample 2 and sample 3 exhibited relatively high FWHM values of 80 cm^{-1} and the intensity ratio $I_{(D)}/I_{(G)}$ was approximately unity. When sample 3 received an exterior load, the consequent spectrum displayed a wider and higher D peak in comparison to the G peak. Obviously, the second-order Raman characteristic changed significantly after sodium expansion and creep deforma-

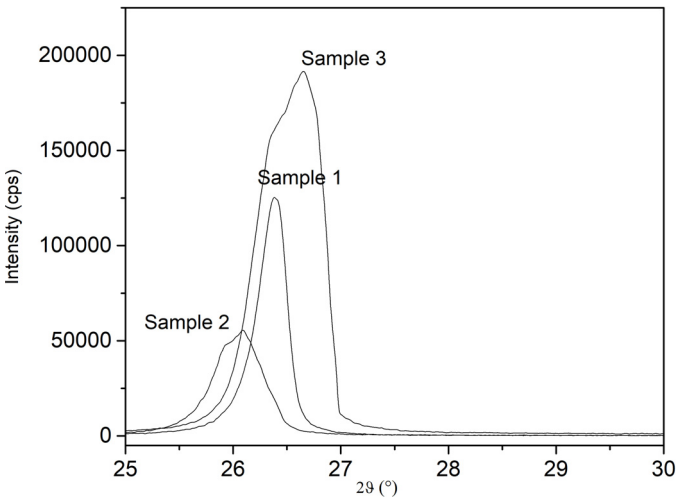

Fig. 3. XRD analysis of the carbon cathode before and after electrolysis

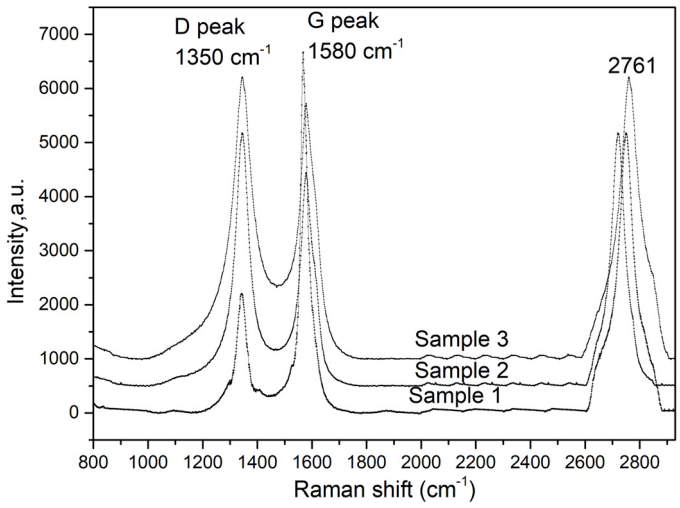

Fig. 4. Raman spectra of the carbon cathode before and after electrolysis

tion resulted in a decrease of the crystal grain and increased the poor order of the sheets along the stacking direction. The variation in phonon correlation length L_a (Å) decreased from 114 Å in the pristine sample to 30 Å for creep deformation. The wave number positions of the 2D bands for sample 3 lied at 2761 cm^{-1}, which was the largest among the tested samples, indicating the layer number of sample 3 sheets was the most. This was aligned with the results of XRD that the decrease of interlayer spacing (d_{002}) invariably resulted in the increase of the layer number of sample 3 sheets per unit thickness.

TABLE 1

Typical quantitative values from Raman spectra of cathode samples

Sample	$I_{(D)}/I_{(G)}$	L_a (Å)	FWHM
1 (pristine)	0.381	114	32
2 (sodium expansion)	1.195	36	61
3 (creep deformation)	1.429	30	74

The rise of the $FWHM_G$ with an increase in the $I_{(D)}/I_{(G)}$ ratio indicates a substantial variation of the Raman spectroscopy during deformation. This was attributed to the disordered crystal structures of carbon and the rise in the disordered areas of the turbulence [19,20]. Fig. 5 shows the extent of structural disordering and induced turbulence in the microstructure. The pristine sample provided the lowest $FWHM_G$ value when compared with the carbon cathode after sodium expansion and creep deformation. This suggests that the pristine sample experienced a lower stress and hence the relatively low stack disordering in the microstructures, which was verified by SEM analysis.

Similar crystal microstructure variations, using both Raman spectra and XRD methods, have been presented for carbon materials under conditions of deformation [21-22], oxidation and purification [23-25]. Furthermore, a substantial increase of the intensity ratio $I_{(D)}/I_{(G)}$ (from 0.381 to 1.195) was observed after the sodium expansion. Thus, sodium penetration into highly crystalline carbon cathodes engenders stress, which results in a structural deterioration such as poor order of the sheets along the stacking direction, kink bands and new boundary development between newly generated microcrystallites.

3.3. Scanning electron microscopy of carbon cathode microstructure

Fig. 5 indicates the surface features of the carbon cathodes. Highly homogeneous and flat regions of primitive graphite sheets oriented with their basal planes are a characteristic of the graphite microstructure. Clearly, the mean particle size was reduced, which correlates well with the increase in the strain (Fig. 2). The surface of the carbon cathodes after deformation was very different from that of the pristine carbon cathode. The morphology of sample 2 (Fig. 5b) showed rippled silk-like waves and flaky pattern with fewer layers representing an expanded microstructure. Cracks were a general characteristic and flakes that were partly stripped (Fig. 5c), developing cavities between

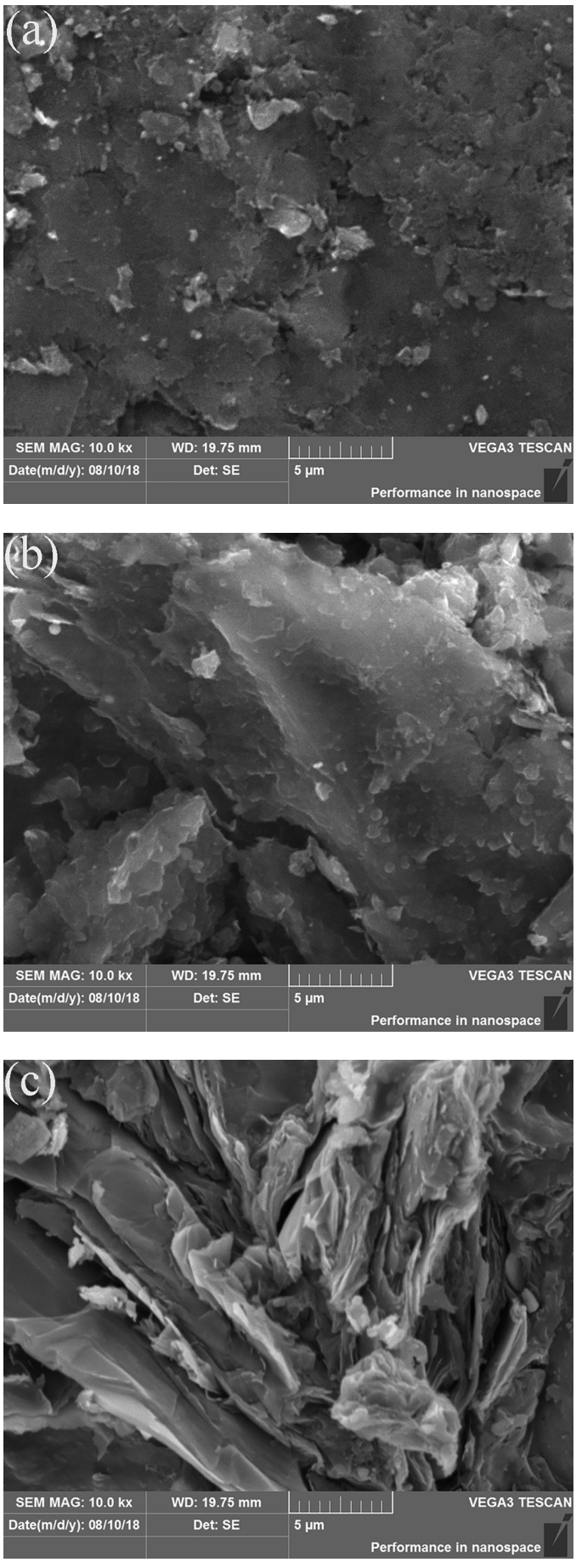

Fig. 5. SEM micrographs of the carbon cathodes. (a) specimen 1, (b) specimen 2, and (c) specimen 3

the layers, which were filled by the sodium and bath. These cavities were the preferred locations for the sodium penetration and intercalation with carbon [26-28]. Furthermore, the development of damage inside the crystal microstructure with increasing stress and distinct structural defects on the surface, such as wrinkling of the graphitic basal layers, twisting and layered stacking faults, were observed. The poorly stacked structure could be susceptible to restructuring, and thus collapses quickly.

Thus, both SEM imaging and Raman spectroscopy proved that substantial mechanical stress evolves during sodium penetration and intercalation with carbon, which injures the crystal structure of these carbon cathodes at the micrometer scale. Such variations provide a reasonable explanation for the sodium expansion and creep deformation of the carbon cathodes. One probable cause is the reduction in the number of places favorable for the sodium and bath penetration, owing to the break-up of graphite sheet and the development of new grain boundaries between the microcrystals, which may not be easy to access to the sodium and bath. These boundaries, caused by the sodium expansion, may offer sites for sodium and bath storage [29].

4. Conclusions

The crystal parameters and microstructure of the cathode samples after deformation were analyzed with SEM and Raman spectroscopy. The results obtained by Raman spectroscopy analysis were consistent with those of SEM, which indicated that both methods were complementary. The techniques provided much evidence that mechanical stress leads to two major types of effects.

The average crystallite size of the cathode graphite reduced with an increase in the extent of deformation during aluminum electrolysis. A marked distinction in Raman spectroscopy was observed between a pristine carbon cathode and carbon cathodes after the sodium expansion and creep deformation. Substantial increases of the intensity ratio $I_{(D)}/I_{(G)}$ and the G-band width were observed with elevated fluence.

The results of XRD analysis and Raman spectroscopy indicated that the layer number of carbon cathode sheets per unit thickness increased with the decrease of the interlayer spacing (d_{002}) during aluminum electrolysis.

The sodium and melts penetration prompted the dislocations rearrangement and crosslinking in the carbon, therefore the carbon structure was deteriorated significantly. With a possible filling of the developed cracks with the sodium and bath, graphite flakes ruptured to smaller, nondirectional pieces. The fragmented layers were scattered randomly but remained within the layer structure normal to the basal planes and the overall stacking was maintained.

Funding

Financial support from National Natural Science Foundation of China (NSFC) (No. U1704154) are gratefully acknowledged.

REFERENCES

[1] M.-A. Coulombe, G. Soucy, L. Rivoaland, L. Davies, Metall. Mater. Trans. B. **47**, 1-16 (2016).
[2] S. Xiao, T. Mokkelbost, O. Paulsen, A.P. Ratvik, G.M. Haarberg, Metall. Mater. Trans. B. **44**, 1311-1316 (2013).
[3] A. Zolochevsky, J. Hop, T. Foosnaes, H. Øye, Carbon. **43**, 1222-1230 (2005).
[4] A. Zolochevsky, J. Hop, G. Servant, T. Foosnaes, H. Øye, Carbon. **41**, 497-505 (2003).
[5] L. Chauke, A.M. Garbers-Craig, Carbon. **58**, 40-45 (2013).
[6] W. Wang, W. Chen, W. Gu, Mat. Sci. Eng. A. **687**, 107--112 (2017).
[7] M.W. Barsoum, A. Murugaiah, S.R. Kalidindi, T. Zhen, Y. Gogotsi, Carbon. **42**, 1435-1445 (2004).
[8] F. Tuinstra, J.L. Koenig, J. Chem. Phys. **53**, 1126-1130 (1970).
[9] D.Y. Wang, C.Y. Wei, M.C. Lin, C.J. Pan, H.L. Chou, H.A. Chen, M. Gong, Y. Wu, C. Yuan, M. Angell, Nature Communications **8**, 1-7 (2017).
[10] R. Krishna, A.N. Jones, L. Mcdermott, B.J. Marsden, J. Nucl. Mater. **467**, 557-565 (2015).
[11] E. Markervich, G. Salitra, M.D. Levi, D. Aurbach, J. Power Sources. **146**, 146-150 (2005).
[12] T. Gruber, T.W. Zerda, M. Gerspacher, Carbon. **32**, 1377-1382 (1994).
[13] Y. Sato, M. Kamo, N. Setaka, Carbon. **16**, 279-280 (1978).
[14] P. Lespade, R. Al-Jishi, M.S. Dresselhaus, Carbon. **20**, 427-431 (1982).
[15] H.N. Zhen, T. Yu, H.L. Yun, Y.W. Ying, P.F. Yuan, Z.X. Shen, Acs. Nano. **2**, 2301-2305 (2008).
[16] V.N. Popov, P. Lambin, Carbon. **54**, 86-93 (2013).
[17] R. Beams, C.L. Gustavo, L. Novotny, J. Phys. Condens Matter. **27**, 1-7 (2015).
[18] T. Priya, N. Dhanalakshmi, S. Thennarasu, N. Thinakaran, Carbohydrate Polymers **197**, 366-374 (2018).
[19] A.C. Ferrari, J. Robertson, Phys. Rev. B Condens. Matter. **61**, 14095-14107 (2000).
[20] M. Huang, H. Yan, T.F. Heinz, J. Hone, Nano Letters. **10**, 4074-4079 (2010).
[21] N.W.B. Balasooriya, P. Touzain, P.W.S.K. Bandaranayake, Ionics. **13**, 305-309 (2007).
[22] E. Asari, Carbon. **38**, 1857-1861 (2000).
[23] S. Osswald, G. Yushin, V. Mochalin, S.O. Kucheyev, Y. Gogotsi, J. Am. Chem. Soc. **128**, 11635-11642 (2006).
[24] Y. Liu, Y. Yang. Renew Energ. **115**, 734-740 (2018).
[25] C. Ban, S Zhu, J. Hou, F. Wang, J. Wang, Z. Jia, J. Zhao. J. Mater. Sci.-Mater. El. **28**, 10992-10996(2017)
[26] N. Adhoum, J. Bouteillon, D. Dumas, J.C. Poignet, Electrochim. Acta. **51**, 5402-5406 (2006).
[27] L. Chauke, A.M. Garbers-Craig, Carbon. **58**, 40-45 (2013).
[28] Z. Fang, N. Gao, X. Li, Q. Liu, M. Liu, Nanoscience & Nanotechnology Letters **8**, 484-491 (2016).
[29] G.K. Simon, T. Goswami, Metall. Mater. Trans. A. **42**, 231-238 (2011)